JBC RESEARCH ARTICLE

Proteasome activator 28γ (PA28γ) allosterically activates trypsin-like proteolysis by binding to the α-ring of the 20S proteasome

Received for publication, March 7, 2022, and in revised form, June 6, 2022 Published, Papers in Press, June 14, 2022,
https://doi.org/10.1016/j.jbc.2022.102140

Taylor A. Thomas[1] **and David M. Smith**[1,2,3,4,*]

From the [1]*Department of Biochemistry, Robert C. Byrd Health Sciences Center, and* [2]*Department of Neuroscience, Robert C. Byrd Health Sciences Center, West Virginia University, Morgantown, West Virginia, USA;* [3]*WVU Rockefeller Neuroscience Institute, Morgantown, West Virginia, USA;* [4]*WVU Cancer Institute, Morgantown, West Virginia, USA*

Edited by George DeMartino

Proteasome activator 28γ (PA28γ/REGγ) is a member of the 11S family of proteasomal regulators that is constitutively expressed in the nucleus and implicated in various diseases, including certain cancers and systemic lupus erythematosus. Despite years of investigation, how PA28γ functions to stimulate proteasomal protein degradation remains unclear. Alternative hypotheses have been proposed for the molecular mechanism of PA28γ, including the following: (1) substrate selection, (2) allosteric upregulation of the trypsin-like (T-L) site, (3) allosteric inhibition of the chymotrypsin-like (CT-L) and caspase-like (C-L) sites, (4) conversion of the CT-L or C-L sites to new T-L sites, and (5) gate opening alone or in combination with a previous hypothesis. Here, by mechanistically decoupling gating effects from active site effects, we unambiguously demonstrate that WT PA28γ allosterically activates the T-L site. We show PA28γ binding increases the Kcat/Km by 13-fold for T-L peptide substrates while having little-to-no effect on hydrolysis kinetics for CT-L or C-L substrates. Furthermore, mutagenesis and domain swaps of PA28γ reveal that it does not select for T-L peptide substrates through either the substrate entry pore or the distal intrinsically disordered region. We also show that a previously reported point mutation can functionally switch PA28γ from a T-L activating to a gate-opening activator in a mutually exclusive fashion. Finally, using cryogenic electron microscopy, we visualized the PA28γ-proteasome complex at 4.3 Å and confirmed its expected quaternary structure. The results of this study provide unambiguous evidence that PA28γ can function by binding the 20S proteasome to allosterically activate the T-L proteolytic site.

Proteasome activator 28γ (PA28γ, also known as Ki antigen, REGγ, PSME3) is a proteasomal activator in the 11S family that is implicated in several cancers (1–3) and rheumatoid arthritis (4) where it is found to be overexpressed. Under normal physiological conditions, PA28γ is constitutively expressed across all tissues (5) and is localized to the nucleus but not within the nucleolus (6). Interestingly, expression of PA28γ has been shown to enhance survival in an *in vitro* model of Huntington's disease (7), and gene therapy of PA28γ improves motor coordination in a murine Huntington's disease model, YAC128 (8). However, in a cell model of spinal and bulbar muscular atrophy, which is caused by polyglutamine (PolyQ) expansion in the androgen receptor, PA28γ had an adverse effect on androgen receptor aggregation in a proteasome-independent manner (9). Despite these physiological and cell biological findings regarding PA28γ's biological roles, the molecular mechanism of how PA28γ stimulates protein degradation by the proteasome remains a mystery.

The 11S family of proteasomal activators extends across all multicellular eukarya and are often interchangeably referred to as PA26/PA28 or REG. This class of activators are all heptameric complexes, ATP-independent and do not contain unfolding or forced translocation activity (10). The 11S family is an expanding class of proteasomal activators found in a variety of species such as *Trypanosoma brucei* (PA26) (11), *Drosophila* (12), *Plasmodium falciparum* (*Pf*)[13], ticks (13), and mammals (10). In mammals, there are three homologs of PA28 within the 11S family: alpha (α), beta (β), and gamma (γ); PA28α and PA28β form an asymmetric heteroheptameric complex known as PA28αβ (14). PA28αβ expression is regulated by interferon-γ and has been identified to play a functional role in major histocompatibility class I antigen presentation (15, 16). In contrast, PA28γ is a homoheptameric complex, that does not form a complex with PA28α or PA28β (10). As described above, PA28γ is implicated in a variety of disease states, but its physiologic role in nuclear proteostasis and how it regulates protein degradation through the proteasome remains unclear. Further, PA26 and PA28αβ complexes have been structurally characterized using X-ray crystallography, and the PA28αβ-immunoproteasome complex has been solved using cryogenic electron microscopy (cryo-EM), but the structure of PA28γ complex remains unknown.

The eukaryotic 20S proteasome is a compartmentalized protease comprised of four heteroheptameric rings in an α, β, β, α arrangement (17, 18). The β rings each contain three

* For correspondence: David M. Smith, dmsmith@hsc.wvu.edu.

active sites and sequesters their protease activity to the hollow interior of the 20S (19). Each active site has unique specificity for amino acid side chains (*i.e.,* β5—chymotrypsin-like [CT-L], β2—trypsin-like [T-L], and β1—caspase-like [C-L]) (20). An α-ring flanks the β rings on either side, and the N termini of the α-subunits fold over the substrate entry pore to form a barrier to the degradation chamber. This barrier is called the proteasomal gate, and it protects the cell from unregulated protein degradation (21). Regulating the proteasomal gate and the precise degradation of cellular substrates is managed by a variety of proteins or protein complexes called proteasomal activators.

Proteasomal activators are highly specialized and have unique functions. Proteasomal ATPases (*i.e.,* regulatory particle or 19S) utilize ATP to recognize, unfold, and translocate substrates into the degradation chamber (22, 23). ATP-independent proteasome activators include PA200/Blm10, PI31, and 11S, each with their own unique regulatory mechanisms. Our current understanding of the 11S-proteasome complex mechanism is based on a novel crystallography study of PA26 in complex with the yeast and archaeal proteasomes, which not only contributed to our understanding of the activation mechanism but also demonstrated the 11S family's capability to activate the proteasome across multiple species (24). Whitby *et al*. revealed that PA26 regulates substrate entry *via* opening the gate of the 20S proteasome. Opening the 20S gate allows peptide substrates to freely defuse through the center of the 11S regulators pore and into the 20S catalytic chamber, where they are degraded. Interestingly a mechanism for stimulating unfolded-protein degradation has not been worked out but is expected to be similar. Recently, two cryo-EM studies substantiated similar mechanisms of proteasomal regulation for PA28αβ and the immunoproteasome and the *Pf*PA28 to 20S complex, indicating that PA26, PA28αβ, and *Pf*PA28 use similar mechanisms to regulate proteasome function (25, 26). In contrast, since its characterization in the 1990s, PA28γ's effect on the 20S proteasome has been under contention. Wilk *et al.* used ammonium sulfate precipitation to purify recombinant PA28γ and concluded that it had 20S gate-opening activity and did not observe activation of a specific proteolytic site (27). Two other groups used a different purification strategy of recombinant PA28γ and also observed gate-opening 20S activity (28, 29). Alternatively, recombinant PA28γ classically purified using ion-exchange and size-exclusion chromatography, N-terminally His-tagged recombinant PA28γ purified using NiNTA resin, and endogenous and transiently overexpressed N-terminally FLAG-tagged PA28γ from cell lines indicates that PA28γ specifically upregulates the cleavage of T-L peptides and does not demonstrate 20S gate opening activity (10, 30). Therefore, as the effect of PA28γ on the 20S proteasome is still widely debated, the specific mechanism has not yet been determined but many could answer this question. A recent cryo-EM structure of human PA200 and human 20S proteasome revealed a unique mechanism of T-L proteolytic activation through switching of the β5 S1 pocket (30), which effectively turns the CT-L site into a T-L site, thus providing a potential mechanism by which T-L peptide hydrolysis could be upregulated by PA28γ. The discovery of this novel mechanism and the long-standing debate of substrate specificity indicates the need to understand the precise mechanism of proteasomal activation by PA28γ. Five alternative hypothesis could explain how PA28γ selectively stimulates T-L peptide hydrolysis: (1) specific substrate selection, (2) allosteric upregulation of T-L catalytic site (T-L site), (3) allosteric inhibition of only the C-L and CT-L catalytic sites, (4) alteration of C-L or CT-L substrate specificity to that of T-L like, or (5) proteasomal gate opening in combination with one of the previous hypothesis (31, 32). However, in previous years, experimentally decoupling the effects PA28γ has on either gate opening, or the catalytic sites would have been very difficult to test as using the constitutive 20S proteasome complicates the analysis due to the potential of gating effects.

The present study was undertaken to rigorously investigate which of these mechanisms PA28γ employs to regulate the proteasome. Understanding the mechanism of this proteolytic stimulation would be important for understanding changes to proteostasis during diseases, such as in cancers where PA28γ expression is upregulated or during Huntington's disease, where the proteasome is inefficient at degrading proteins with poly-glutamine expanded repeats, which are primarily degraded by the T-L site (33). To investigate the mechanism of PA28γ's proteasomal regulation, we employed the α3ΔN-20S or "open-channel" proteasome. α3ΔN is a mutant proteasome species that has an N terminal, 10-residue truncation of the α3 subunit. The α3 N termini stabilizes the closed state of the proteasome by interacting with α2 and α4 in the 20S pore. Thus, the α3N-terminal deletion produces a proteasome that has a constitutively open channel (21). Combining the α3ΔN-20S with PA28γ allows us to mechanistically decouple proteasomal gate-opening from potential allosteric activation of a protease site. This combined with other protein engineering tools allows for the rigorous determination of mechanisms that PA28γ employs to regulate substrate degradation *via* the proteasome.

Results

WT PA28γ demonstrates upregulation of T-L catalytic activity

Before specifically asking which hypothesis PA28γ uses to activate 20S function, we first sought to validate the activity of our purified recombinant PA28γ, as previous groups indicated different PA28γ functions that were deemed to be dependent on the specific purification strategy employed (27, 34). As controls, we also purified recombinant PA28αβ, which is known to induce gate-opening, and a mutant of PA28γ that has been reported to switch its activity. This prior study showed that a lysine mutation on the third helix of PA28γ, K188 to E (PA28γ-K188E), switched PA28γ's activation activity from T-L activating to proteasomal gate-opening, thus causing it to function like PA28αβ (31) (Fig. 1*A*). Our recombinant human PA28γ in the presence of human 20S proteasome (H20S) induces an almost 20-fold increase in proteolytic activity for the T-L proteolytic site-specific peptide

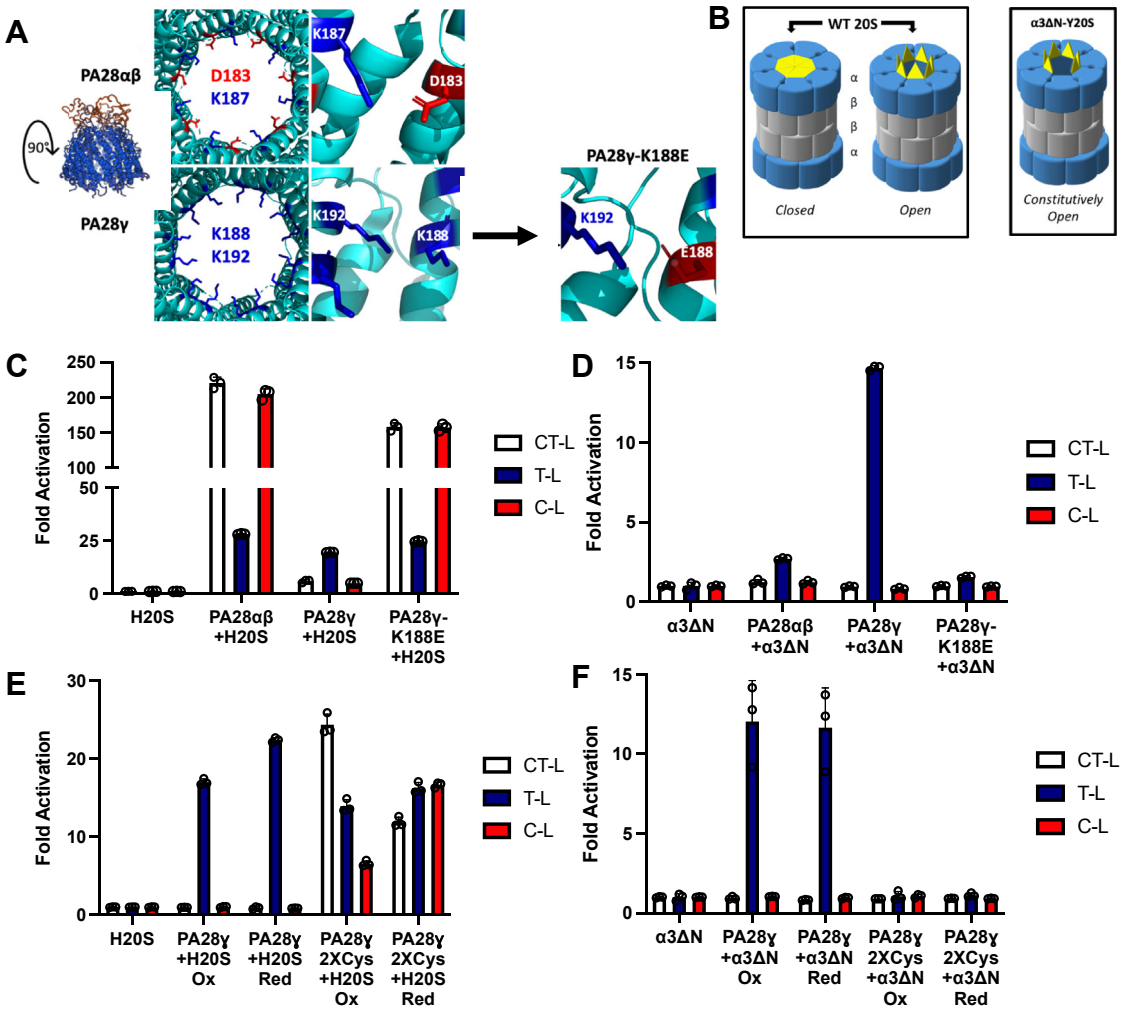

Figure 1. PA28γ stimulation of T-L activity does not require 20S gate-opening. *A*, substrate entry pore of PA28αβ (PDB: 5MX5) alternates positive and negative charges around the ring, whereas PA28γ contains a positive substrate entry pore. PA28γ mutant, PA28γ-K188E, was generated to create a pore more like PA28αβ (PA28γ structures based on modified PDB: 5MX5). *B*, the WT 20S proteasome can fluctuate between a closed and open state due to thermodynamic flux, the closed state protects substrates from nonspecific entry. The constitutively active, open channel α3ΔN-Y20S-proteasome has an N terminal truncation mutation that causes the gate to remain open and allows nonspecific substrate entry. *C*, purified H20S proteasome (1 nM) activity was measured for all three proteolytic sites (RFU/min) in the presence of recombinant PA28αβ (50 nM), PA28γ or PA28γ-K188E (62.5 nM). *D*, purified constitutively open-gate α3ΔN-Y20S (0.1 nM) activity was measured for all three proteolytic sites (RFU/min) in the presence of recombinant PA28αβ (50 nM), PA28γ or PA28γ-K188E (62.5 nM). *E*, H20S (1 nM) activity was measured for all three proteolytic sites (RFU/min) in the presence of PA28γ or PA28γ2XCys (62.5 nM) under reducing and oxidizing conditions. *F*, purified constitutively open-gate α3ΔN-Y20S (0.1 nM) activity was measured for all three proteolytic sites (RFU/min) in the presence of recombinant PA28γ or PA28γ2XCys (62.5 nM) under reducing and oxidizing conditions. Experiments were controlled for using buffer identical to the proteasomal activator. Results are the mean of at least three independent experiments performed in triplicate (error bars represent SD) normalized to the average of the H20S or α3ΔN-Y20S control. C-L, caspase-like; CT-L, chymotrypsin-like; H20S, human 20S proteasome; PA28γ, proteasome activator 28γ; T-L, trypsin-like.

substrate (RLR-AMC) when compared to H20S only controls (Fig. 1*C*), as was similarly reported in Gao *et al* (34). However, under the same conditions, PA28αβ and PA28γ-K188E stimulated substantial proteolytic activity for all peptide substrates, rather than only T-L activity (Fig. 1*C*). These results replicate past observations that the PA28γ-K188E mutation alters PA28γ activity and likely switches it to a gate-opening form (similar to PA28αβ). This is because gate opening is expected to stimulate the degradation of all peptides regardless of their proteolytic site specificity, as it should freely allow the entry of all peptide substrates. These results clearly demonstrate that PA28γ stimulates the proteasome differently than PA28αβ and that the K188E mutation alters how it stimulates 20S function. These results can be explained by several possible mechanisms used by PA28γ that are listed in the introduction. It is also not clear from these results alone if WT PA28γ can function *via* both gate-opening and T-L–like activation or if these mechanisms could function mutually exclusively in WT PA28γ.

To test whether PA28γ directly upregulates the T-L proteolytic site or performs substrate-selective gate opening, we purified α3ΔN proteasomes from yeast (α3ΔN-Y20S). α3ΔN-Y20S has an N-terminal truncation mutation to the α3 subunit of the Y20S that alleviates the closed gate conformation induced by the N termini of the WT Y20S α-subunits (35) (Fig. 1*B*). Importantly, WT yeast 20S respond similarly to activation by PA28αβ and PA28γ as do human 20S (Fig. S1).

The α3ΔN-Y20S thus mechanistically decouples gating effects from proteolytic site effects allowing us to unambiguously determine if PA28γ alters proteolytic site activity in the absence of gating contributions. We hypothesized that if an 11S family member's proteasomal regulatory mechanism was to open the gate, there would be no change from the α3ΔN-Y20S control, as the proteasome is already constitutively active (*i.e.,* peptide substrates are free to defuse into the 20S without hinderance). However, if the activator's regulatory mechanism included allosteric changes to the proteolytic sites, this could be clearly observed enzymatically in the absence of a functioning gate. Our results demonstrate that there were no changes to the fold activation of α3ΔN-Y20S in the presence of PA28αβ and PA28γ-K188E (Fig. 1*D*), which demonstrates and confirms that PA28αβ and PA28γ-K188E indeed function to open the proteasomal gate allowing peptide to diffuse in and do not themselves affect the activity of proteolytic sites. However, PA28γ induced ∼15-fold activation of the α3ΔN-Y20S in the presence of the T-L substrate RLR-AMC, when compared to the α3ΔN-Y20S controls and did not inhibit or alter the degradation of CT-L or C-L substrates (LLVY-AMC and nLPnLD-AMC) (Fig. 1*D*). It is important to note that the cleavage rates of the peptide substrates vary between each peptide and that the T-L peptide, RLR-AMC, has the lowest V_{max} when compared to the CT-L and C-L peptides (36). These differences will be further analyzed below and in the discussion. These results demonstrate that PA28γ activates T-L activity of the proteasome without requiring the induction of gate-opening, but further alternative mechanisms must be ruled out to determine if this activation is catalytically allosteric. These results also conclusively demonstrate that a single point mutation is indeed capable to switch PA28γ from a T-L activation state to gate-opening state, and that these two states are mutually exclusive, as K188E mutant could not activate the α3ΔN-Y20S.

Disulfide crosslinking has been established to be a useful tool in studying proteasomal activators' structure and function, particularly for homomers, such as the archaeal proteasomal AAA+ ATPase, PAN (37). Briefly, cysteine point mutations are strategically induced into the protein subunit that will interact with the point mutation in the neighboring subunits. We hypothesized that if the two interacting lysine residues on helix 3 are important for maintaining PA28γ T-L activity and if the gate-opening state is the result of the lysine-glutamate salt bridge interactions in PA28γ-K188E and PA28αβ, then inducing two hydrophobic residues, like cysteine, would also change the activity of PA28γ from T-L stimulating to gate opening. We adopted the previous approach for PA28γ and induced two cysteine point mutations at the K188 and K192 positions within helix 3, which will further be called PA28γ2XCys, similar to the K188 to E mutation (Fig. 1*A*). When tested in a proteasome activity assay using WT H20S or α3ΔN-Y20S, the results reveal that PA28γ2XCys has similar activity patterns to that of PA28γ-K188E or PA28αβ and opens the proteasomal gate without inducing T-L activation (Fig. 1, *E* and *F*). As cysteine residues can form disulfide bonds, we tested these mutants under both reducing, noncrosslinked and oxidizing, crosslinked conditions. Under both conditions, PA28γ2XCys stimulated all three activities in the WT 20S but did not stimulate the open channel 20S indicating that it induces only gate opening. One caveat is that PA28γ2XCys did not stimulate gate-opening as well as did PA28γK1888E, presumably due to a less efficient conformational state induced by changing hydrophilic pore residues to hydrophobic ones. Nevertheless, these results further demonstrate that pore stabilizing mutations in PA28γ, whether salt-bridge, hydrophobic, or covalent in nature, can switch PA28γ from an allosteric activating state to a gate-opening state.

PA28γ does not alter the specificity of the CT-L or C-L proteolytic sites to upregulate T-L activity

While intuitively one would think that an increase in T-L like activity is likely due to an increase in the proteolytic activity of the T-L proteolytic site, this may not necessarily be the case. A recent cryo- EM study of the human PA200-20S complex determined that PA200's upregulation of T-L activity is the result of conformational changes to the S1 pocket of the β5 subunit to change from CT-L activity to T-L activity (30). Therefore, we asked if it was possible PA28γ was using a similar mechanism to upregulate T-L activity. We hypothesized that if PA28γ caused allosteric changes to the β5 S1 binding pocket to increase T-L activity, then inhibiting the CT-L site prior to binding of PA28γ would block PA28γ ability to stimulate T-L activity. Alternatively, if PA28γ allosterically upregulates T-L activity or is selective for T-L peptide substrates, we should see loss of that activity in the presence of a T-L inhibitor. Therefore, we employed the use of proteasome inhibitors epoxomicin (irreversible inhibitor) and leupeptin that specifically target the catalytic sites of β5 and β2, respectively (36). We began the experiment by incubating the H20S with the inhibitor prior to running the proteasome activity assay. Upon completion of the assay, we normalized the data to the H20S controls without the inhibitor to determine the impact of proteolytic activation with and without the inhibitor. Treatment with epoxomicin caused 95 to 100% inhibition of CT-L activity in the absence and presence of all indicated 11S activators using the CT-L substrate, LLVY-AMC (Fig. 2*A*). However, PA28γ stimulation of the T-L substrate, RLR-AMC, was essentially unaffected in the presence of epoxomicin. Alternatively, in the presence of the β2 inhibitor, leupeptin, our data demonstrated that T-L activity was diminished 94 to 100% in the absence or presence of all the indicated 11S activators, including PA28γ where activity went from 30-fold stimulation (Fig. 2*A*) to no stimulation (Fig. 2*B*). Our results definitively show that PA28γ's ability to activate T-L activity does not require a functional CT-L site and cannot simulate T-L activity if the T-L–like site is inhibited. Therefore, PA28γ does not function by altering CT-L catalytic activity, as has been suggested for the PA200 activator.

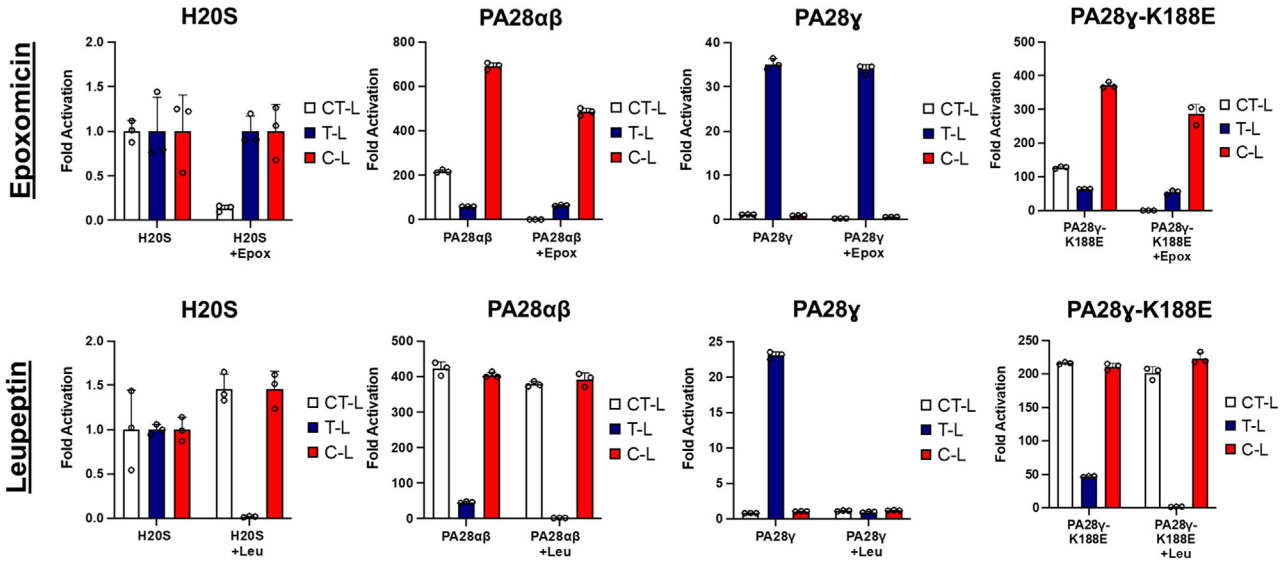

Figure 2. PA28γ does not change the specificity of other proteolytic sites to upregulate T-L activity. Purified H20S proteasomes were incubated with inhibitor [epoxomicin (100 nM) or leupeptin (40 μM)] and recombinant PA28αβ (50 nM), PA28γ or PA28γ-K188E (62.5 nM) were subsequently added to individual experiments. Proteasome activity was recorded for all proteolytic sites (RFU/min). Experiments were controlled for using buffer identical to the respective inhibitor. Results are the mean of at least three independent experiments performed in triplicate (error bars represent SD) normalized to the average of the H20S control. C-L, caspase-like; CT-L, chymotrypsin-like; H20S, human 20S proteasome; PA28γ, proteasome activator 28γ; T-L, trypsin-like.

PA28γ changes the K_m and V_{max} of T-L peptides for α3ΔN-Y20S

The results from our inhibitor data led us to ask the question of how PA28γ or PA28αβ changes proteolytic activity for each active site. To answer this question, we wanted to monitor the kinetic changes of each proteolytic site in the presence of either PA28γ or PA28αβ. Using the α3ΔN-Y20S, we were able to effectively answer this question as we can directly decouple the effects of activator binding and gate-opening from changes to the proteolytic sites. We performed dose responses of CT-L (LLVY-AMC), T-L (RLR-AMC), and C-L (nLPnLD-AMC) peptides to monitor kinetic changes of α3ΔN-Y20S proteolysis in the presence of either PA28γ or PA28αβ. Compared to the α3ΔN-Y20S controls, PA28αβ demonstrated negligible changes to the K_m or V_{max} for any of the three peptide substrates (Fig. 3). This observation further demonstrates that PA28αβ does not allosterically alter the proteolytic sites but functions solely as a gate-opening proteasomal activator. Alternatively, PA28γ does not modify the K_m or V_{max} for CT-L or C-L peptide substrates but does substantially change the K_m and V_{max} of the T-L substrate RLR-AMC. The presence of PA28γ decreases the K_m by >400% and increases the V_{max} by >300%. This equates to a >13-fold increase in the catalytic efficiency (K_{cat}/K_m) of the T-L site by PA28γ. These results demonstrate that binding of PA28γ to the 20S increases both the catalytic affinity and the maximum proteolytic rate of the T-L site, without affecting the CT-L– or C-L–like activities. Therefore, PA28γ can use a nongating activation mechanism, which is mechanistically distinct from PA28αβ. While it is tempting to speculate that these results strongly suggest allosteric activation of the T-L site, similar results could possibly be obtained if PA28γ allowed the passage of some peptide substrates differently than others to function as a substrate filter or sieve based on peptide charge. We will investigate this last alternative mechanism next.

PA28γ does not select for substrates via its charged intrinsically disordered region or charged substrate entry pore

The above results indicate that PA28γ can upregulate T-L activity by a nongating mechanism, but what remains unclear is whether PA28γ functions to exclude entry of some but not other substrates from the proteasome whereby, it could specifically allow entry of T-L peptide substrates (38). All of the 11S/PA28 family members have an intrinsically disordered region (IDR), that has also been referred to as their homolog-specific insert, that is located around the substrate entry pore of the 11S complex and opposite of the proteasome-binding interface (38, 39). To answer if PA28γ can filter some peptide substrates, we designed two PA28γ variants that altered the IDR domain. The first replaced the IDR of PA28γ with the IDR of PA28α, the second variant removed the entire IDR of PA28γ and replaced it with a small linker region sufficient to ensure formation of proper quaternary structure. We therefore created two PA28γ mutants, PA28γ-α and PA28γΔIDR. PA28γ-α is the PA28γ variant that contains the IDR from PA28α (*i.e.,* it swaps IDR domains). A PA28α-γ swap was also created but did not heptamerize under our conditions and so could not be analyzed. The PA28γΔIDR is a deletion of PA28γ's IDR but includes an 8-residue serine–glycine linker to limit the introduction of steric hinderance that a complete loss of the IDR would likely cause. When we tested the ability of these two PA28γ variants to activate 20S function, we found that both the PA28γ-α and PA28γΔIDR upregulated T-L substrate degradation, similar to WT PA28γ, for both H20S and α3ΔN-Y20S. In addition, these two IDR variants showed

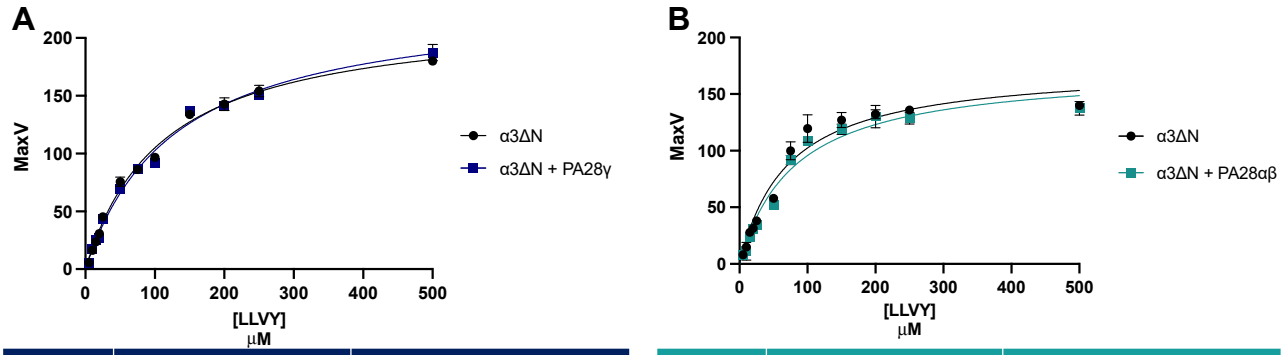

	α3ΔN	PA28γ + α3ΔN
V_{max}	221.7 (212.3-231.9)	234.3 (222.8-246.9)
K_m	111.2 (99.73-124.0)	128.6 (114.0-145.1)

	α3ΔN	PA28αβ + α3ΔN
V_{max}	174.8 (162.0-189.1)	170.3 (158.9-183.1)
K_m	70.68 (57.0-87.68)	79.35(65.58-96.08)

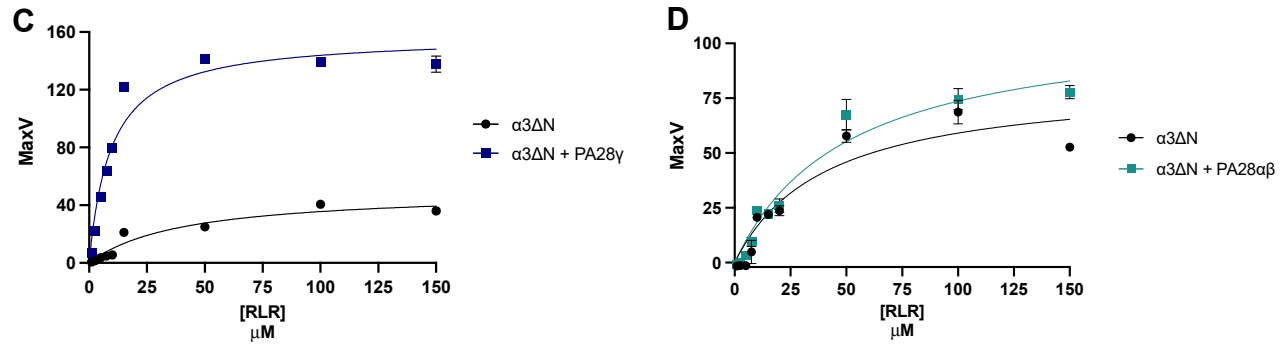

	α3ΔN	PA28γ + α3ΔN
V_{max}	50.03 (42.72-60.36)	157.3 (146.7-168.5)
K_m	40.60 (26.69-65.11)	9.414 (7.469-11.81)

	α3ΔN	PA28αβ + α3ΔN
V_{max}	82.94 (69.22-101.5)	109.7 (95.96-127.5)
K_m	40.36 (26.09-64.81)	49.51 (36.15-69.62)

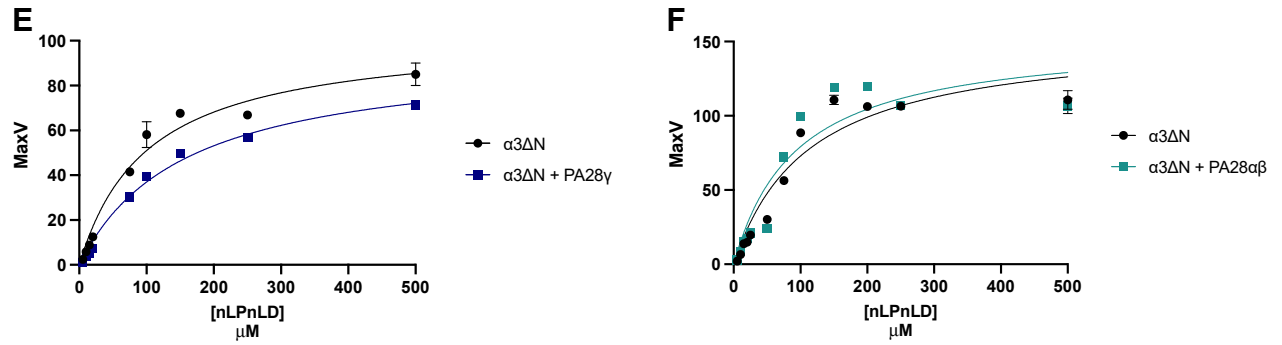

	α3ΔN	PA28γ + α3ΔN
V_{max}	102.8 (93.54-113.4)	94.65 (88.49-101.6)
K_m	101.5 (78.71-131.0)	156.1 (133.4-183.1)

	α3ΔN	PA28αβ + α3ΔN
V_{max}	152.0 (133.7-174.4)	153.4 (132.7-178.9)
K_m	103.2(74.72-143.0)	93.71 (64.66-136.2)

Figure 3. PA28γ changes the K_m and V_{max} of T-L peptides for α3ΔN-Y20S. Dose responses of peptide substrates were performed with α3ΔN-Y20S (0.1 nM) and either PA28αβ (50 nM) or PA28γ (62.5 nM). Dose responses are as follows: (*A*) PA28γ and LLVY-AMC (0–500 μM), (*B*) PA28αβ and LLVY-AMC (0–500 μM), (*C*) PA28γ and RLR-AMC (0–150 μM), (*D*) PA28αβ and RLR-AMC (0–150 μM), (*E*) PA28γ and nLPnLD-AMC (0–500 μM), and (*F*) PA28αβ and nLPnLD-AMC (0–500 μM). All experiments are the mean of three independent experiments (error bars represent SD). 95% CI is denoted following all values in parenthesis. PA28γ, proteasome activator 28γ; T-L, trypsin-like.

no change in activity for the C-L or CT-L substrates in the presence of either H20S or α3ΔN-Y20S, also similar to WT PA28γ (Fig. 4, *B* and *C*). Based on these results, we can conclude that PA28γ's T-L activation mechanism does not require its IDR domain, and thus this domain must also not confer any peptide "filtering" capacity. In addition, the IDR domain from PA28α does not confer any gate opening activity to PA28γ when swapped.

As discussed previously, PA28γ-K188E has a substrate entry pore that mimics the substrate entry pore of PA28αβ and

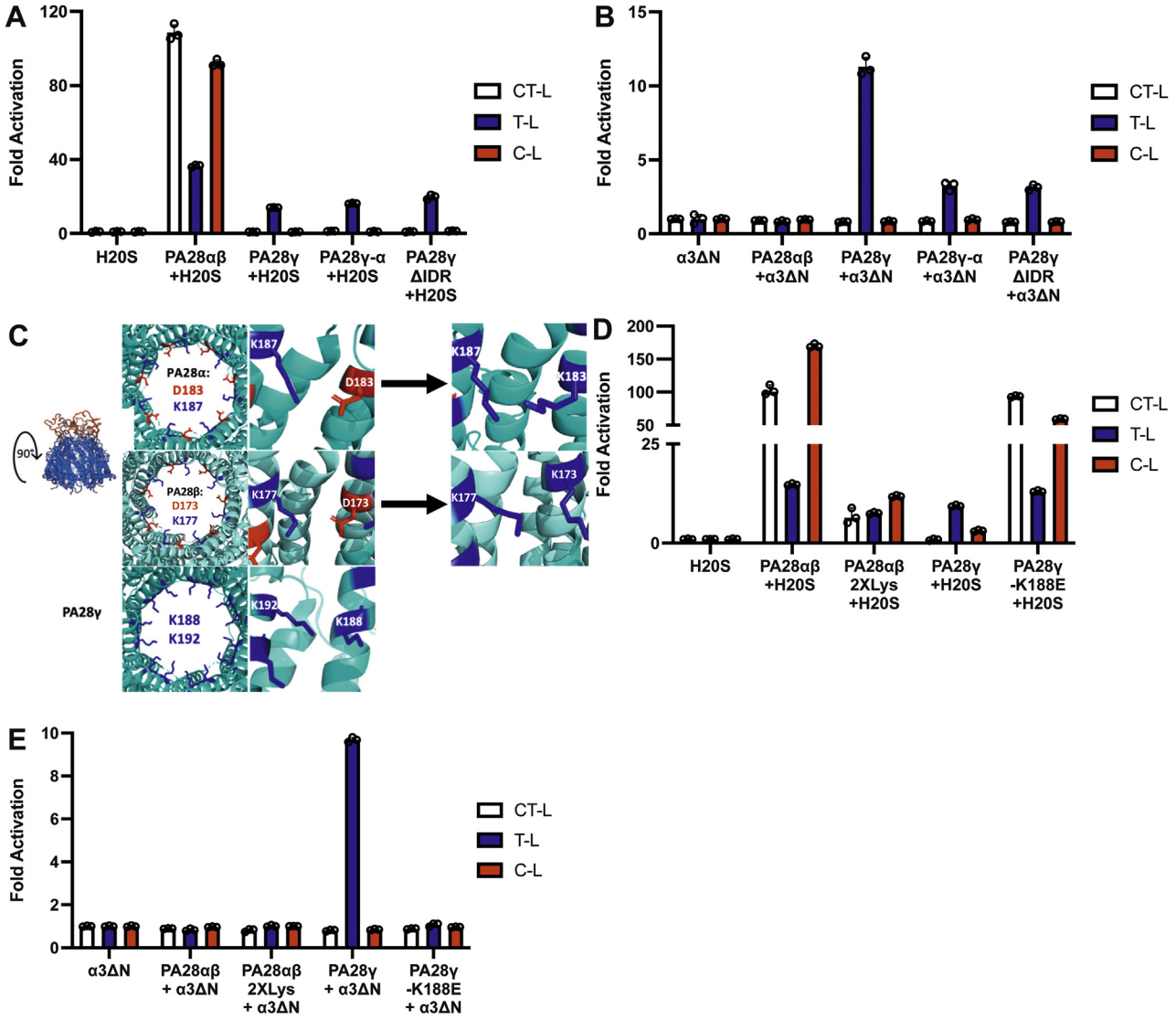

Figure 4. PA28γ does not select for substrates *via* its intrinsically disordered region or substrate entry pore. *A*, purified H20S proteasome (1 nM) activity was measured for all three proteolytic sites (RFU/min) in the presence of recombinant PA28αβ (50 nM), PA28γ, PA28γ-α, or PA28γΔIDR (62.5 nM). *B*, purified constitutively open-gate α3ΔN-Y20S (0.1 nM) activity was measured for all three proteolytic sites (RFU/min) in the presence of recombinant PA28αβ (50 nM), PA28γ, PA28γ-α, or PA28γΔIDR (62.5 nM). *C*, site-directed mutagenesis was used to create the PA28αβ mutant, PA28αβ2XLys, a substrate entry pore mutant that maintains positive charges around the ring, like PA28γ. (PDB: 5MX5—PA28α and 5MSK—PA28β; PA28γ structures based on modified PDB: 5MX5) *D*, purified H20S proteasome (1 nM) activity was measured for all three proteolytic sites (RFU/min) in the presence of recombinant PA28αβ, PA28αβ2XLys (50 nM), PA28γ, or PA28γ-K188E (62.5 nM). *E*, purified constitutively open-gate α3ΔN-Y20S (0.1 nM) activity was measured for all three proteolytic sites (RFU/min) in the presence of recombinant PA28αβ, PA28αβ2XLys (50 nM), PA28γ, or PA28γ-K188E (62.5 nM). All experiments are the mean of three independent experiments (error bars represent SD) normalized to the average of the H20S or α3ΔN-Y20S control. C-L, caspase-like; CT-L, chymotrypsin-like; H20S, human 20S proteasome; PA28γ, proteasome activator 28γ; T-L, trypsin-like.

changes the functional mechanism of PA28γ from allosteric activation to gate-opening (Fig. 1*A*). We therefore asked the question if the charges in this pore region could affect which types of peptides are able to pass through PA28αβ. To ask this question, we introduced point mutations into PA28αβ that would mimic the charges in the substrate entry pore of PA28γ. We then asked if these mutations would be sufficient to switch PA28αβ′s activity to that of PA28γ. This experiment was performed for two reasons: (1) to test whether PA28αβ and PA28γ can filter peptide substrates through their substrate entry pores and (2) to implicate helix 3 in the unique functional activity of PA28αβ and PA28γ on the 20S proteasome. As PA28αβ has two separate subunits, we created this mutant by inducing point mutations in helix 3 of PA28α-D183K and PA28β-D173K, which will further be called PA28αβ2XLys (Fig. 4*C*). A proteasome activity assay using WT H20S revealed that PA28αβ2XLys still stimulates the degradation of all three types of substrates though at a reduced capacity: approximately 2- to 10-fold less activity amongst all peptide substrates when compared to WT PA28αβ (Fig. 4*D*). Nevertheless, these results demonstrate that PA28αβ2XLys is functional to induce gate opening but importantly does not selectively prevent the passage of some types of peptides, despite its very different pore charges. To confirm this conclusion, we also found that PA28αβ2XLys was unable to stimulate peptide hydrolysis in the α3ΔN-Y20S at any capacity (similar to WT PA28αβ),

which also indicates that PA28αβ2XLys maintains its gate opening ability (Fig. 4*E*) but does not "filter" substrates based on their charge. This result reveals that the generation of a completely positively charged pore in PA28αβ was not able to switch it to a T-L activating complex (like PA28γ), thus demonstrating that differences in pore charge are unable to selectively exclude some types of peptides from entering the degradation chamber. One caveat of this experiment is that mutagenesis of helix 3 in PA28αβ diminished the activator's ability to induce gate-opening, but it did not change its general function. Based on the structure of PA28γ, there are three different regions where peptide passage through PA28γ and entry into the 20S could be affected: (1) the IDR, (2) the substrate entry pore, and (3) the proteasome gate. We have generated mutants in all three of these locations and found that none of them could change the effect that PA28γ has on the proteasome. Therefore, these results clearly demonstrate that PA28γ does not select for peptide substrates through its IDR or its substrate entry pore and does not specifically open the proteasomal gate for T-L peptide substrates, but in fact, allosterically upregulates the catalytic capacity of the β2 subunits, thus increasing T-L–specific peptide proteolysis.

Cryo-EM electron density reveals structural topology of PA28γ

Recently, the structures of various 11S family members have been solved using cryo-EM and X-ray crystallography (25, 40, 41). However, the structure of the PA28γ complex or the PA28γ-20S proteasome complex has remained undetermined. Using cryo-EM, we were able to generate a low-resolution reconstruction of the human PA28γ-20S complex to 4.3Å (Fig. 5*A*). This electron density reveals that PA28γ binds to the 20S proteasome using its C termini to dock into the proteasomal intersubunit pockets of the α-ring, like PA26 (42) and PA28 (25, 41) activators (Fig. S2). Further, when we overlay our electron density with the recent structure of the PA28αβ-immunoproteasome complex, it is clear that PA28γ adopts an overall topology and quaternary structure that is similar to PA28αβ (Fig. 5*C*). The tertiary and secondary structures of PA28αβ and PA28γ also align similarly relative to one another (Fig. 5, *D* and *E*). Figure 5*E* also shows a slice through the PA28γ map that includes the PA28αβ model, and it is clear the helix 3 (center most helix) occupies similar space in both homologs. Interestingly, our structure reveals a density in the pore of PA28γ that does not appear in the model of PA28αβ (Fig. 5, *B* and *D*). This cryo-EM structural reveals that PA28γ adopts a similar tertiary conformation to the fellow mammalian homolog, PA28αβ, even though PA28γ only has 42.1% sequence identity to PA28α and 33.6% identity with PA28β, and even though both activators activate proteasome function in very different ways.

Discussion

This study unambiguously demonstrates that within the 11S family, PA28γ and PA28αβ can use two completely different mechanisms to activate proteasome function. Previous work initially determined that PA28γ could stimulate the degradation of T-L substrates but did not explicitly define how it achieves its function. Based on previous literature and structure/function analysis, five potential mechanisms were proposed that could answer how PA28γ upregulated T-L peptide

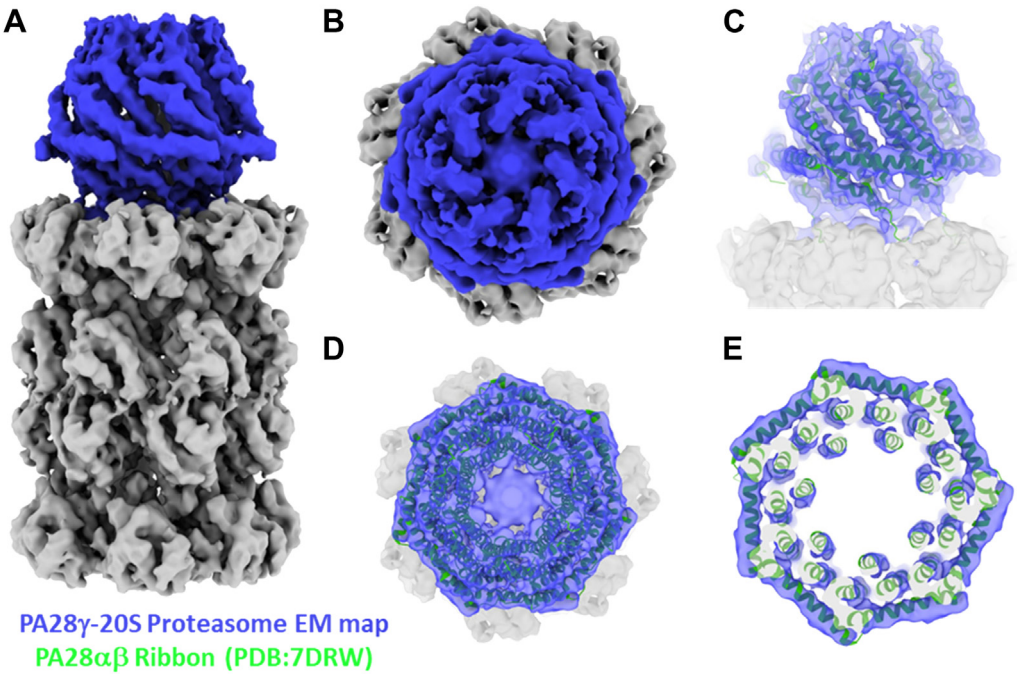

Figure 5. Cryo-EM reveals PA28γ has a similar structure to other 11S regulators when bound to the 20S proteasome. *A*, full 4.3 Å electron density of the human PA28γ-20S proteasome complex after density modification. PA28γ density is colored *blue*, and the 20S densities are colored *gray*. C7 symmetry was applied during 3D reconstruction since PA28γ is a homoheptamer. *B*, top-down view of the substrate entry pore of PA28γ. *C*, molecular model of PA28αβ (PDB: 7DRW) fit into the electron density of the PA28γ-20S complex (side view). *D*, top view of C. *E*, same as D except the map and model are cropped through the 7-fold symmetry axis to focus on the helix 3 density (center most helix). PA28γ, proteasome activator 28γ.

degradation: (1) specific substrate selection, (2) allosteric upregulation of the T-L catalytic site, (3) allosteric inhibition of the CT-L and C-L catalytic sites, (4) conversion of the CT-L or C-L sites to new T-L catalytic sites, and (5) gate-opening in combination with a previous hypothesis. Our results effectively ruled out mechanism 1 that the PA28γ could function as a substrate selective "sieve" and allow only entry of only peptide substrates with positive charges. The "sieve" model would require that PA28γ is able to open the 20S gate, but only allow entry of select peptides (*e.g.,* T-L peptides). Further, if PA28γ functioned as a "sieve", it would also limit CT-L and C-L peptides from entering the proteasome, which would appear as inhibition in the open channel 20S. Our results from Figure 1*D* clearly demonstrate that PA28γ upregulates the degradation of the T-L peptide but did not inhibit the degradation of CT-L or C-L peptides in the constitutively active proteasome. Moreover, it is reasonable to assume that if PA28γ was using a sieve model, that the IDR surrounding the substrate entry pore may play a role in substrate selection. Figure 4 clearly shows that mutagenesis to the IDR does not affect PA28γ's ability to upregulate the proteolysis of T-L peptide substrates. In addition, mutation of PA28αβ's pore to generate a ring of positive lysine's mimicking PA28γ's pore (Fig. 4, *C–E*) demonstrated that this 2XLys mutation did not confer any "sieving-like" properties to PA28αβ and did not change how it activated 20S function. These results clearly rule out contributions from mechanism 1 for PA28γ function. None of our experiments could rule out mechanism 2—allosteric activation of the T-L like site. Mechanism 3 or allosterically inhibition of CT-L or C-L activity (combine with gate-opening—mechanism 5) to increase T-L degradation is ruled out by Figure 1 showing that T-L activity is still stimulated even when the gate is constitutively open, and CT-L and C-L activity are not affected in the open mutant. In addition, Figure 3, *A* and *E* show that the equilibrium kinetics of CT-L and C-L peptides remain unchanged when PA28γ is bound to open channel protesasome complex demonstrating that PA28γ cannot inhibit these active sites (Fig. 3*C* serves as a control to show that PA28γ does indeed bind to the open channel 20S in these conditions). Together, Figure 3 conclusively demonstrated that in the absence of a functioning 20S gate, PA28γ increased the catalytic affinity (K_m) and increased the V_{max} of the T-L like site for RLR-AMC (Fig. 3*C*), inducing a 13-fold increase in catalytic efficiency of the T-L site. These results suggest that PA28γ can allosterically activate the T-L proteolytic site. Mechanism 4 is ruled out by results shown in Figure 2 that support that PA28γ does not switch the CT-L site to be more T-L. These experiments demonstrate that PA28γ's ability to upregulate T-L peptide degradation was unaffected even when the CT-L site was modified with a covalent inhibitor, revealing that PA28γ could not switch the CT-L site to T-L, as has been suggested for PA200's mechanism of T-L–like activation. In addition, we further verified that pretreatment with a T-L inhibitor could indeed inhibit PA28γ's ability to upregulate T-L activity. Finally, the fact that PA28γ's ability to upregulate T-L peptide degradation occurs with WT or open channel mutant 20S (Fig. 1, *C* and *D*) demonstrates that it does not need to induce gate opening to stimulate T-L activity (ruling out mechanism 5). Taken together, our results clearly demonstrate that PA28γ, through long-range interactions (Fig. 6*A*), can allosterically affect the β2 subunits of the 20S proteasome to upregulate its T-L enzymatic activity. These results suggest that one biological function of PA28γ in the nucleus could be to upregulate the T-L catalytic activity of β2, as it has been shown that even with the highest affinity peptide substrates catalysis of T-L substrates is far lower than that of C-L or CT-L substrates (43) (Figs. 1*C* and 3). This increased β2 processivity could aid in the degradation of DNA binding proteins that often have a high density of positive charge. Interestingly, it is not understood how PA28γ influences the T-L catalytic site of the immunoproteasome, despite extensive research on the PA28αβ-immunoproteasome complex. It is known that immune function is not impacted when PA28γ is knocked out (44). In addition, since the cellular localization of the immunoproteasome is under contention and seemingly cell specific (45, 46), it is not clear if it could colocalize with the nuclear PA28γ. However, if PA28γ does bind to immunoproteasomes that contain β2i subunits, we could not predict what the affect could be since B2 is substantially different from β2i, as they only share a 58.3% identity.

WT PA28γ has two basic residues on helix 3 (K188 and K192), while WT PA28αβ has a basic (lysine) and acidic (aspartate) residue in the homologous positions of PA28α (D183 and K187) and PA28β (D173 and K177; Figs. 1 and 6). The structures of PA28αβ reveal that the basic residue in helix 3 interacts with the acidic residue in helix 3 of the neighboring subunit (14), which would effectively induce a repeating salt-bridge around the substrate entry pore that could theoretically stabilize the substrate entry pore and the 11S structure in general. We hypothesize that the rigidity within the substrate entry pore, due to stabilizing salt bridges, could somewhat lock PA28αβ (and other similar gate-opening 11S regulators) into a conformation that would allow for the activation loops to more effectively impose their symmetry onto the α-subunits of the 20S to cause gate-opening as has been proposed for PA26 (41). Here, we clearly show that PA28αβ's only function is to induce gate opening since it could not affect open channel 20S activity. Contrarily, PA28γ's helix 3 provides repeating positive charges that surround the substrate entry pore, which is expected to generate repulsive forces that reduce pore stability and create a more dynamic or flexible 11S activator. In support of this notion, the K188E mutation in PA28γ introduces stabilizing interactions to the helix 3 ring, which switches PA28γ's function to gate-opening (Figs. 1, 4, and 6). We further probed these helix 3 interactions and switching mechanism by generating the PA28γ2XCys mutant, which contains two hydrophobics in the K188 and K192 positions. This variant similarly switches PA28γ from T-L activating to gate-opening (whether disulfide crosslinked or not). Therefore, two different mutations that increase the interactions of helix 3 with neighboring helix 3's likely increase helix 3 positional stability in the pore, and this causes PA28γ to switch into a gate-opening state. In contrast, when we destabilized the substrate entry pore of PA28αβ with our PA28αβ2XLys

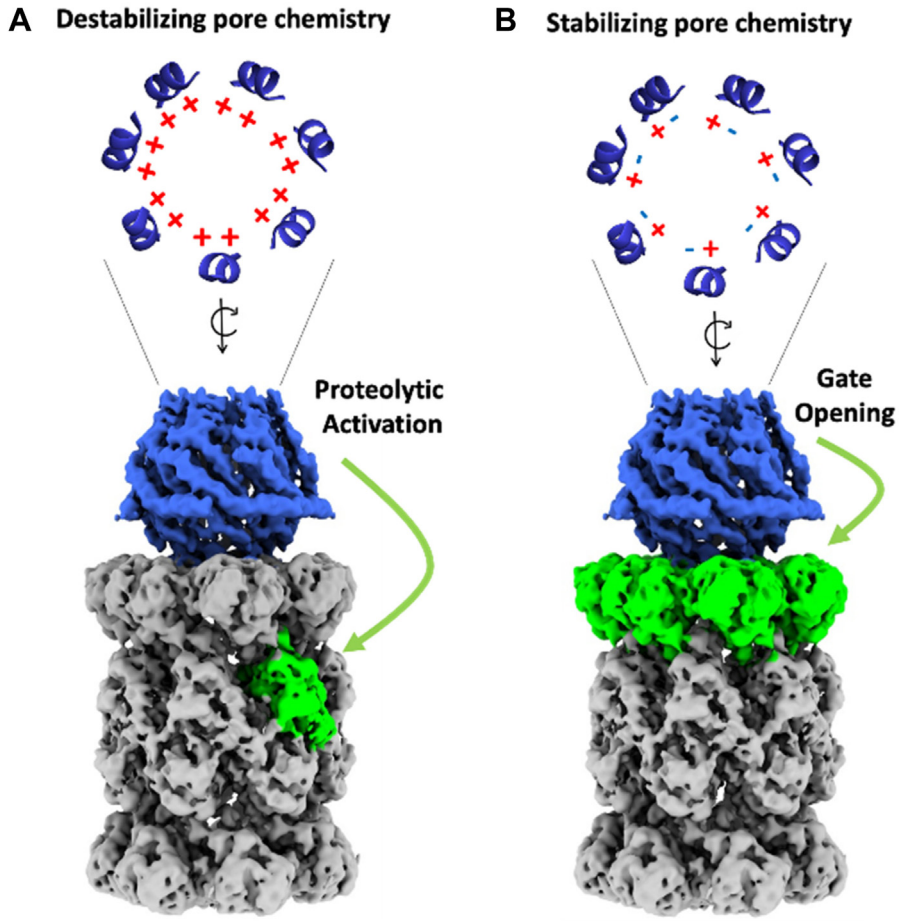

Figure 6. Model of PA28γ and PA28γ-K188E pore charges and their effects on the 20S proteasome. Proteasomal regulation by PA28γ is directly affected by helix 3 interactions. *A*, WT PA28γ has a positively charged (*i.e.,* helix 3 repelling), substrate entry pore which allosterically induces proteolytic activation of the T-L proteolytic site in the 20S proteasome. *B*, A single point mutation (K188E) to PA28γ creates an ionically stabilized (helix 3 interacting) substrate entry pore that alternates positive and negative charges similar to PA28αβ. Replacing these charges with hydrophobic residues functions similarly. This changes the regulatory mechanism of PA28γ causing to switch its function to one that induce proteasomal gate opening. These conclusions are based on PA28γ's ability to affect the activity as the open channel 20S proteasome, which can dissociate gating affects from active site affects. PA28γ, proteasome activator 28γ; T-L, trypsin-like.

mutant, we saw a marked reduction in gate-opening activity (mirroring PA28γ activity) when compared to WT PA28αβ, but it did not induce a complete functional switch like the PA28γ-K188E mutant did, meaning it did not induce T-L activity (Fig. 4*D*). This indicates that there must be other differences between PA28αβ and PA28γ that compensate for their mechanistic differences besides pore stability. Although mutations that increase helix 3 interactions in the pore of PA28γ can cause it to switch activity, it is not known if WT PA28γ, under physiological conditions, can similarly switch states as part of its normal function to degrade proteins, though it is tempting to speculate that this switching mechanism could be a component of how it regulates protein degradation, which is currently not understood.

Based on our observations, we hypothesize that PA28γ's positively charged substrate entry pore allows it to adopt a conformational that can generate the long-range allosteric effects that allow it to activate the 20S T-L site. In support of this notion, a recent study by Lesne *et al.* used hydrogen-deuterium exchange coupled to mass spectrometry to determine that PA28αβ and PA28γ adopt different conformations when binding the proteasome, as the activation loops and helix 1 of PA28αβ were heavily protected from hydrogen-deuterium solvent exchange when bound to the proteasome compared to PA28γ (47). Our structure of the human PA28γ-20S complex reveal that PA28γ adopts a quaternary topology similar to other structurally characterized 11S regulators (*i.e.,* PA26, PA28*Pf,* and PA28αβ). Further, the overall structure of the PA28γ-20S proteasome complex revealed that PA28γ docks its C termini into the intersubunit pockets of the proteasome's α-ring, a mechanism paralleled by other 11S regulators, and does not bind the β ring directly to upregulate T-L proteolysis. We also revealed a density unique to PA28γ that occupies the substrate entry pore. It is expected that this density is its IDR, and although we could not resolve this region, it supports the idea that this region is highly disordered. Our structure allows us to visually conclude that PA28γ in general has many overall qualities that align with the 11S family of regulators. While the application of C7 symmetry to the PA28γ-20S complex is reasonable and useful since PA28γ is a homoheptamer, the same symmetry application to the heteroheptomeric 20S averages out its pseudosymmetry, thus causing loss of

asymmetric structural information, which would be required to observe structural changes in the β2 subunits. Unfortunately, the particle number obtained was too low for 3D reconstruction without symmetry application. Lesne *et al.*'s hydrogen-deuterium exchange coupled to mass spectrometry study complements our biochemical results and supports our hypothesis that PA28γ uses a distinct proteasomal activation mechanism from other 11S regulators, while structurally preserving similar tertiary and quaternary protein structures.

The PA28γ-20S complex has recently been demonstrated to degrade unfolded proteins (29) and is known to play a role in nuclear processes such as: cell cycle progression and cell proliferation (44, 48), apoptosis (48), formation of nuclear speckles (49), and DNA repair (50). Within these processes, PA28γ-20S complex has also been demonstrated to facilitate the degradation of many nuclear proteins, such as SRC-3/AIB1 (51), c-Myc (52), p21 (53), hepatitis C virus (54), and MDM2 (55). Interestingly, many PA28γ substrates appear to be DNA binding proteins. In addition to cancer progression, PA28γ could also play a role in protecting against some neurodegenerative diseases, like Huntington's disease, which is caused by expression and accumulation of the PolyQ expanded Huntington protein (56). A prior study using PolyQ expanded peptide substrates determined that the T-L site was responsible for PolyQ substrate degradation, and longer PolyQ expanded repeats (30 Q amino acids) were unable to be degraded by the mammalian proteasome (33). While further studies showed that the proteasome could cleave PolyQ proteins (57), it is clear from both studies that PolyQ cleavage is very slow. Based on these results, it seems that PA28γ's ability to stimulate the T-L site would be expected to play an important role in accelerating the degradation of polyglutamine proteins, which could be protective. In support of this notion, treatment with PA28γ has been shown to have a protective effect in PolyQ neurodegenerative disease studies (7, 8). Therefore, understanding how PA28γ enhances the proteolytic activity of the T-L site as shown here would provide a mechanistic understanding and platform to design drugs that could be used to potentially treat Huntington's disease. Therefore, based on our results and this literature, we hypothesize that the role of PA28γ in proteasomal nuclear proteostasis is to enhance the T-L activity of the 20S proteasome for more effective degradation of positively charged proteins, which are often DNA and RNA binding proteins. This proposed function of the PA28γ-20S complex could explain why some cancers upregulate PA28γ, as it could facilitate the expeditious degradation of important transcription factors and ubiquitination cascade proteins. This function could also answer the question of why PA28γ overexpression in PolyQ neurodegenerative disease rescues the disease phenotype. This study lays the groundwork to better understand the mechanism of how PA28γ activates T-L activity, which could inform efforts to design inhibitors of PA28γ function that could be used to specifically treat PA28γ-overexpressed cancers and 20S proteasome T-L site stimulating drugs that could be used to treat PolyQ neurodegenerative diseases.

Experimental procedures

Proteasome purifications

Bovine 20S (B20S) proteasomes were purified from bovine liver as described (58). Liver was homogenized, cleared, and passed over weak anion exchange resin (DE52, GE Life Sciences). B20S proteasomes were eluted using a stepwise NaCl gradient. Fractions with proteolytic activity were pooled and dialyzed before strong anion exchange (Resource Q, GE Life Sciences) separation using a linear NaCl gradient. Elution with significant suc-LLVY-AMC activity were pooled and further separated using a hydroxyapatite chromatography column (CHT-I, Bio-Rad) using a linear KPO_4 gradient. Eluted fractions with significant proteolytic activity were pooled and dialyzed, and B20S purity (>95%) was determined using SDS-PAGE and densitometry (ImageJ, NIH). Concentration was determined using a Bradford assay with bovine serum albumin as the reference protein. Eukaryotic α3ΔN-Y20S were expressed and purified from yeast using anion exchange chromatography, as described with minor modifications (43) Briefly, size-exchange chromatography (SEC) (Superose six Increase, GE Life Sciences) was performed on pooled fractions with proteolytic activity after Resource Q. H20S proteasomes were purified from stably transfected HEK 293T cells, as previously described (59).

Proteasome activator purifications

PA28αβ was purified as described (60). Briefly, recombinant PA28αβ was expressed in BL21-STAR *E.* coli and purified using strong anion exchange (HiTrapQ and MonoQ, GE Life Sciences), followed by hydroxyapatite (CHT-II, Bio-Rad), and finished with SEC (Superose 6 Increase, GE Life Sciences). Recombinant PA28γ was expressed in Rosetta *E. coli* and purified using Ni-NTA affinity resin (Qiagen) and followed with SEC (Superose 6 Increase, GE Life Sciences), as previously described (10). PA28γ-K188E was created using QuikChangeII Site Directed Mutagenesis Kit (Agilent) and purified using methods like PA28γ, as previously described (31). PA28γ-α, PA28γ-2XCys, PA28αβ2XLys, and PA28γΔIDR constructs were designed as G-Blocks with N-terminal 6XHis Tags (Integrated DNA Technologies) and cloned into pET11a plasmids. pET11a plasmids with successfully cloned G-blocks were transformed into BL21-STAR *E. coli* and purified using the PA28γ Ni-NTA purification methods. Concentrations were determined using a Bradford assay with bovine serum albumin as the reference protein.

Proteasome activity assays

Unless otherwise stated, B20S (1 nM), Y20S (1 nM), H20S (1 nM), and α3ΔN-Y20S (1 nM) were all assayed using fluorogenic peptides, as previously described (36), using a Biotek 96-well plate reader. Briefly, 20S proteasomes were incubated in a reaction buffer containing 50 mM Tris-HCL (pH 7.5), 5% glycerol, 1 mM DTT, and 100 μM fluorogenic substrate (suc-LLVY-AMC, boc-RLR-AMC, boc-LRR-AMC, Ac-nLPnLD-AMC or Z-LLE-AMC) and put into a 96- half well black

flat-bottomed treated plate. 20S proteasomes were subsequently treated with either PA28αβ (50 nM), PA28γ (62.5 nM), PA28γ-K188E (62.5 nM), PA28αβ2XLys (50 nM), PA28γ-α (62.5 nM), or PA28γΔIDR (62.5 nM). Fluorescence measurements were taken every 30s for 60 min (ex/em: 380/460 nm). The slope of the linear increase in fluorescence is directly proportional to the rate of 20S proteasome activity. Assays in the presence of proteasomal activators are normalized to the 20s proteasome only control. All molar concentrations of the proteins above are based on the molecular weight of the total complex.

Proteasome inhibitor assays

Assays were performed under reaction conditions and protein concentrations similar to proteasome activity assays. B20S proteasomes were incubated in reaction buffer with either PA28αβ, PA28γ, or PA28γ-K188E, and either epoximicin (100 nM) or leupeptin (40 μM) was subsequently added (epoximicin, Enzo Life Sciences; leupeptin, Sigma Aldrich). Assays were controlled for using replicates without inhibitors read simultaneously.

Substrate dose responses

Dose response assays were done following a modified proteasome activity assay protocol. Briefly, α3ΔN-Y20S (1 nM) was put into a proteasome activity assay buffer alone or with either PA28αβ (50 nM) or PA28γ (62.5 nM). Fluorogenic substrate was added in a dose-dependent manner (suc-LLVY-AMC: 0–500 μM; boc-RLR-AMC: 0–200 or 225 μM; ac-nLPnLD-AMC: 0–500 μM). Assays were analyzed for the MaxV at each concentration, and dose responses were analyzed using GraphPad Prism9. The fold change (FC) in catalytic efficiency (K_{CAT}/K_M) was calculated as FC in V_{MAX}/K_M because $K_{CAT} = V_{MAX}/[E]$, and the [E] was the same in both conditions used to calculate FC.

Oxidation/reduction assay

WT PA28γ and PA28γ2XCys were assayed using a modified protocol (37). Briefly, WT PA28γ and PA28γ2XCys were incubated in 0.1% β-mercaptoethanol for 1 h before being desalted using a Zeba Spin Desalting Column (Thermo Scientific). Proteins were then incubated at 37 °C for 10 min in 0.1% β-mercaptoethanol or tetrathionate (1 mM) to reduce or oxidize the cysteines, respectively. After incubation, proteins were added to a proteasome activity assay master mix, previous protocol was followed.

Cryo-EM sample preparation and data collection

Copper Quantifoil R 1.2/1.3300 mesh (EMS) grids were cleaned and treated with amylamine using a PELCO easiGlow Glow Discharge cleaning system. PA28γ and H20S were mixed at a 1:1 M ratio, and 3 uL of the sample mixture was placed onto a grid. Grid was subsequently blotted by hand using blotting paper and immediately flash frozen in liquid ethane using a manual plunge freeze apparatus. Data collection was done using a Titan Krios transmission electron microscope (Thermo Fisher) operated at 300 kW and a magnification of x81,000, which resulted in 1.08 Å/px. Images were collected using a Falcon IIIEC direct electron detector camera equipped with a K3/GIF system operating in counting and super resolution modes. Electron dose per pixel of 50 e-/$Å^2$ was saved as a movie with each movie being dose fractioned into 40 frames within a target defocus range of -2.5 to -1.25. All data were collected using cryoSPARC software (Thermo Fisher).

Cryo-EM single particle analysis

Two thousand three hundred twenty-eight total movies were collected, and we used 2300 for structural determination. Single particle analysis of the PA28γ-20S proteasome complex was done using cryoSPARC (Fig. S3). All images were aligned and summed using motion correction. After contrast transfer function estimation using cryoSPARC's patch-based contrast transfer function estimator, 31,712 particles were autopicked from the micrographs and subjected to several rounds of 2D classification to get rid of junk particles (Fig. S3*B*). Three thousand three hundred fifty eight particles primarily side view orientation (Fig. S3*E*) from single and double cap in PA28 years-20S 2D classes were used to generate five ab-initio models to further remove junk particles (Fig. S3*C*). One of the resulting ab-initio models produced a PA28 years-20S complex from 876 particles, which were used for homogeneous regiment for 3D classification with C7 symmetry applied using the map from prior determined ab-into model (Fig. S3, *C* and *D*). The gold standard (0.143) Fourier shell correlation resolution was calculated form 2 half maps (Cryosparc) to be 4.3 Å (Fig. S3*F*). All representations of the PA28γ-20S proteasome complex were created using UCSF ChimeraX (61).

Data availability

Data are available in the manuscript. Cryo-EM data are available in the EMDB under entry ID EMD-26379 (Deposition ID: D_1000261262).

Supporting information—This article contains supporting information (Figs. S1–S3).

Acknowledgments—Transmission electron micrographs were recorded at the University of Virginia Molecular Electron Microscopy Core facility (RRID:SCR_019031), which is supported in part by the School of Medicine and built with NIH grant G20-RR31199. In addition, the Titan Krios (S10-RR025067), Falcon II/3EC direct detector (S10-OD018149), and K3/GIF (U24-GM116790) were purchased in part or in full with the designated NIH grants. Molecular graphics and analyses performed with UCSF ChimeraX, developed by the Resource for Biocomputing, Visualization, and Informatics at the University of California, San Francisco, with support from National Institutes of Health R01-GM129325 and the Office of Cyber Infrastructure and Computational Biology, National Institute of Allergy and Infectious Diseases.

Author contribution—T. T. investigation; T. T. formal analysis; T. T. writing-original draft; D. M. S. supervision; T. T. and D. M. S.

conceptualization; T. T. and D. M. S. methodology; T. T. and D. M. S. data curation; T. T. and D. M. S. writing-review and editing.

Funding and additional information—This work was supported by NIH-R01GM107129 to D. M. S.

Conflict of interest—The authors declare that they have no conflicts of interest with the contents of this article.

Abbreviations—The abbreviations used are: B20S, bovine 20S; cryo-EM, cryogenic electron microscopy; CT-L, chymotrypsin-like; C-L, caspase-like; FC, fold change; H20S, human 20S proteasome; IDR, intrinsically disordered region; PA28γ, proteasome activator 28γ; PolyQ, polyglutamine; SEC, size-exchange chromatography; T-L, trypsin-like.

References

1. Okamura, T., Taniguchi, S. I., Ohkura, T., Yoshida, A., Shimizu, H., Sakai, M., *et al.* (2003) Abnormally high expression of proteasome activator-γ in thyroid neoplasm. *J. Clin. Endocrinol. Metab.* **88**, 1374–1383
2. Wang, X., Tu, S., Tan, J., Tian, T., Ran, L., Rodier, J.-F., *et al.* (2011) REG gamma: a potential marker in breast cancer and effect on cell cycle and proliferation of breast cancer cell. *Med. Oncol.* **28**, 31–41
3. He, J., Cui, L., Zeng, Y., Wang, G., Zhou, P., Yang, Y., *et al.* (2012) REGγ is associated with multiple oncogenic pathways in human cancers. *BMC Cancer* **12**, 75
4. Gruner, M., Moncsek, A., Rödiger, S., Kühnhardt, D., Feist, E., and Stohwasser, R. (2014) Increased proteasome activator 28 gamma (PA28γ) levels are unspecific but correlate with disease activity in rheumatoid arthritis. *BMC Musculoskelet. Disord.* **15**, 1–10
5. Noda, C., Tanahashi, N., Shimbara, N., Hendil, K. B., and Tanaka, K. (2000) Tissue distribution of constitutive proteasomes, immunoproteasomes, and PA28 in rats. *Biochem. Biophys. Res. Commun.* **277**, 348–354
6. Soza, A., Knuehl, C., Groettrup, M., Henklein, P., Tanaka, K., and Kloetzel, P.-M. (1997) Expression and subcellular localization of mouse 20S proteasome activator complex PA28. *FEBS Lett.* **413**, 27–34
7. Seo, H., Sonntag, K.-C., Kim, W., Cattaneo, E., and Isacson, O. (2007) Proteasome activator enhances survival of Huntington's disease neuronal model cells. *PLoS One* **2**, e238
8. Jeon, J., Kim, W., Jang, J., Isacson, O., and Seo, H. (2016) Gene therapy by proteasome activator, PA28γ, improves motor coordination and proteasome function in Huntington's disease YAC128 mice. *Neuroscience* **324**, 20–28
9. Yersak, J. M., Montie, H. L., Chevalier-Larsen, E. S., Liu, Y., Huang, L., Rechsteiner, M., *et al.* (2017) The 11s proteasomal activator regγ impacts polyglutamine-expanded androgen receptor aggregation and motor neuron viability through distinct mechanisms. *Front. Mol. Neurosci.* **10**, 1–14
10. Realini, C., Jensen, C. C., Zhang, Z. G., Johnston, S. C., Knowlton, J. R., Hill, C. P., *et al.* (1997) Characterization of recombinant REGα, REGβ, and REGγ proteasome activators. *J. Biol. Chem.* **272**, 25483–25492
11. Yao, Y., Huang, L., Krutchinsky, A., Wong, M. L., Standing, K. G., Burlingame, A. L., *et al.* (1999) Structural and functional characterizations of the proteasome-activating protein PA26 from Trypanosoma brucei. *J. Biol. Chem.* **274**, 33921–33930
12. Masson, P., Andersson, O., Petersen, U.-M., and Young, P. (2001) Identification and characterization of a drosophila nuclear proteasome regulator a homolog of human 11 S REGgamma (PA28gamma). *J. Biol. Chem.* **276**, 1383–1390
13. Paesen, G. C., and Nuttall, P. A. (1996) A tick homologue of the human Ki nuclear autoantigen. *Biochim. Biophys. Acta* **1309**, 9–13
14. Huber, E. M., and Groll, M. (2017) The mammalian proteasome activator PA28 forms an asymmetric a4b3 complex. *Structure* **25**, 1–8
15. Dick, T. P., Ruppert, T., Groettrup, M., Kloetzel, P. M., Kuehn, L., Koszinowski, U. H., *et al.* (1996) Coordinated dual cleavages induced by the proteasome regulator PA28 lead to dominant MHC ligands. *Cell* **86**, 253–262
16. Früh, K., and Yang, Y. (1999) Antigen presentation by MHC class I and its regulation by interferon γ. *Curr. Opin. Immunol.* **11**, 76–81
17. Groll, M., Ditzel, L., Löwe, J., Stock, D., Bochtler, M., Bartunik, H. D., *et al.* (1997) Structure of 20S proteasome from yeast at 2.4 Å resolution. *Nature* **386**, 463–471
18. Hegerl, R., Pfeifer, G., Pühler, G., Dahlmann, B., and Baumeister, W. (1991) The three-dimensional structure of proteasomes from Thermoplasma acidophilum as determined by electron microscopy using random conical tilting. *FEBS Lett.* **283**, 117–121
19. Groll, M., and Huber, R. (2003) Substrate access and processing by the 20S proteasome core particle. *Int. J. Biochem. Cell Biol.* **35**, 606–616
20. Kisselev, A. F., Akopian, T. N., Woo, K. M., and Goldberg, A. L. (1999) The sizes of peptides generated from protein by mammalian 26 and 20 S proteasomes. Implications for understanding the degradative mechanism and antigen presentation. *J. Biol. Chem.* **274**, 3363–3371
21. Groll, M., Glickman, M. H., Finley, D., Bajorek, M., Köhler, A., Moroder, L., *et al.* (2000) A gated channel into the proteasome core particle. *Nat. Struct. Biol.* **7**, 1062–1067
22. Schweitzer, A., Aufderheide, A., Rudack, T., Beck, F., Pfeifer, G., Plitzko, J. M., *et al.* (2016) Structure of the human 26S proteasome at a resolution of 3.9 Å. *Proc. Natl. Acad. Sci. U. S. A.* **113**, 7816–7821
23. preprint de la Peña, A. H., Goodall, E. A., Gates, S. N., Lander, G. C., and Martin, A. (2018) Structures-engaged 26S proteasome reveal the mechanisms for ATP hydrolysis-driven translocation. *bioRxiv*. https://doi.org/10.1101/393223
24. Whitby, F. G., Masters, E. I., Kramer, L., Knowlton, J. R., Yao, Y., Wang, C. C., *et al.* (2000) Structural basis for the activation of 20S proteasomes by 11S regulators. *Nature* **408**, 115–120
25. Xie, S. C., Metcalfe, R. D., Hanssen, E., Yang, T., Gillett, D. L., Leis, A. P., *et al.* (2019) The structure of the PA28–20S proteasome complex from Plasmodium falciparum and implications for proteostasis. *Nat. Microbiol.* **4**, 1990–2000
26. Chen, J., Wang, Y., Xu, C., Peng, C., and Ding, Z. (2020) Cryo-EM of mammalian PA28 ab -iCP immunoproteasome reveals a distinct mechanism of proteasome activation by PA28 αβ. *Nat. Commun.* **12**, 739
27. Wilk, S., Chen, W. E., and Magnusson, R. P. (2000) Properties of the nuclear proteasome activator PA28γ (REGγ). *Arch. Biochem. Biophys.* **383**, 265–271
28. Jonik-Nowak, B., Menneteau, T., Fesquet, D., Baldin, V., Bonne-Andrea, C., Méchali, F., *et al.* (2018) PIP30/FAM192A is a novel regulator of the nuclear proteasome activator PA28γ. *Proc. Natl. Acad. Sci. U. S A.* **115**, E6477–E6486
29. Frayssinhes, J.-Y. A., Cerruti, F., Laulin, J., Cattaneo, A., Bachi, A., Apcher, S., *et al.* (2021) PA28γ-20S proteasome is a proteolytic complex committed to degrade unfolded proteins. *Cell Mol. Life Sci.* **79**, 45
30. Toste Rêgo, A., and da Fonseca, P. C. A. (2019) Characterization of fully recombinant human 20S and 20S-PA200 proteasome complexes. *Mol. Cell* **76**, 138–147.e5
31. Li, J., Gao, X., Ortega, J., Nazif, T., Joss, L., Bogyo, M., *et al.* (2001) Lysine 188 substitutions convert the pattern of proteasome activation by REGgamma to that of REGs alpha and beta. *EMBO J.* **20**, 3359–3369
32. Cascio, P. (2021) Pa28γ: new insights on an ancient proteasome activator. *Biomolecules* **11**, 228
33. Venkatraman, P., Wetzel, R., Tanaka, M., Nukina, N., and Goldberg, A. L. (2004) Eukaryotic proteasomes cannot digest polyglutamine sequences and release them during degradation of polyglutamine-containing proteins. *Mol. Cell* **14**, 95–104
34. Gao, X., Li, J., Pratt, G., Wilk, S., and Rechsteiner, M. (2004) Purification procedures determine the proteasome activation properties of REGγ (PA28γ). *Arch. Biochem. Biophys.* **425**, 158–164
35. Groll, M., Bajorek, M., Köhler, A., Moroder, L., Rubin, D. M., Huber, R., *et al.* (2000) A gated channel into the proteasome core particle. *Nat. Struct. Biol.* **7**, 1062–1067
36. Kisselev, A. F., Callard, A., and Goldberg, A. L. (2006) Importance of the different proteolytic sites of the proteasome and the efficacy of inhibitors varies with the protein substrate. *J. Biol. Chem.* **281**, 8582–8590

37. Snoberger, A., Brettrager, E. J., and Smith, D. M. (2018) Conformational switching in the coiled-coil domains of a proteasomal ATPase regulates substrate processing. *Nat. Commun.* **9**, 2374
38. Zhang, Z., Realini, C., Clawson, A., Endicott, S., and Rechsteiner, M. (1998) Proteasome activation by REG molecules lacking homolog-specific inserts. *J. Biol. Chem.* **273**, 9501–9509
39. Zhang, Z., Clawson, A., Realini, C., Jensen, C. C., Knowlton, J. R., Hill, C. P., *et al.* (1998) Identification of an activation region in the proteasome activator REGalpha. *Proc. Natl. Acad. Sci. U. S. A.* **95**, 2807–2811
40. Huber, E. M., and Groll, M. (2017) The mammalian proteasome activator PA28 forms an asymmetric α4β3 complex. *Structure* **25**, 1473–1480.e3
41. Chen, J., Wang, Y., Xu, C., Chen, K., Zhao, Q., Wang, S., *et al.* (2021) Cryo-EM of mammalian PA28αβ-iCP immunoproteasome reveals a distinct mechanism of proteasome activation by PA28αβ. *Nat. Commun.* **12**, 1–12
42. Förster, A., Masters, E. I., Whitby, F. G., Robinson, H., and Hill, C. P. (2005) The 1.9 A structure of a proteasome-11S activator complex and implications for proteasome-PAN/PA700 interactions. *Mol. Cell* **18**, 589–599
43. Kisselev, A. F., Kaganovich, D., and Goldberg, A. L. (2002) Binding of hydrophobic peptides to several non-catalytic sites promotes peptide hydrolysis by all active sites of 20 S proteasomes. Evidence for peptide-induced channel opening in the alpha-rings. *J. Biol. Chem.* **277**, 22260–22270
44. Barton, L., Runnels, H., Schell, T., Cho, Y., Tevethia, S., Deepe, G., Jr., *et al.* (2004) Deficient mice γ activator immune defects in 28-kDa proteasome. *J. Immunol.* **172**, 3948–3954
45. Petersen, A., and Zetterberg, M. (2016) The immunoproteasome in human lens epithelial cells during oxidative stress. *Invest. Ophthalmol. Vis. Sci.* **57**, 5038–5045
46. van Scheppingen, J., Broekaart, D. W. M., Scholl, T., Zuidberg, M. R. J., Anink, J. J., Spliet, W. G., *et al.* (2016) Dysregulation of the (immuno) proteasome pathway in malformations of cortical development. *J. Neuroinflammation* **13**, 1–16
47. Lesne, J., Locard-Paulet, M., Parra, J., Zivković, D., Menneteau, T., Bousquet, M.-P., *et al.* (2020) Conformational maps of human 20S proteasomes reveal PA28-and immuno-dependent inter-ring crosstalks. *Nat. Commun.* **11**, 6140
48. Murata, S., Kawahara, H., Tohma, S., Yamamoto, K., Kasahara, M., Nabeshima, Y., *et al.* (1999) Growth retardation in mice lacking the proteasome activator PA28gamma. *J. Biol. Chem.* **274**, 38211–38215
49. Baldin, V., Militello, M., Thomas, Y., Doucet, C., Fic, W., Boireau, S., *et al.* (2008) A novel role for PA28-proteasome in nuclear speckle organization and SR protein trafficking. *Mol. Biol. Cell* **19**, 1706–1716
50. Levy-Barda, A., Lerenthal, Y., Davis, A. J., Chung, Y. M., Essers, J., Shao, Z., *et al.* (2011) Involvement of the nuclear proteasome activator PA28γ in the cellular response to DNA double-strand breaks. *Cell Cycle* **10**, 4300
51. Li, X., Lonard, D. M., Jung, S. Y., Malovannaya, A., Feng, Q., Qin, J., *et al.* (2006) The SRC-3/AIB1 coactivator is degraded in a ubiquitin- and ATP-independent manner by the REGγ proteasome. *Cell* **124**, 381–392
52. Chen, X., Barton, L. F., Chi, Y., Clurman, B. E., and Roberts, J. M. (2007) Ubiquitin-independent degradation of cell-cycle inhibitors by the REGγ proteasome. *Mol. Cell* **26**, 843–852
53. Li, X., Amazit, L., Long, W., Lonard, D. M., Monaco, J. J., and O'Malley, B. W. (2007) Ubiquitin- and ATP-independent proteolytic turnover of p21 by the regγ-proteasome pathway. *Mol. Cell* **26**, 831–842
54. Moriishi, K., Mochizuki, R., Moriya, K., Miyamoto, H., Mori, Y., Abe, T., *et al.* (2007) Critical role of PA28γ in hepatitis C virus-associated steatogenesis and hepatocarcinogenesis. *Proc. Natl. Acad. Sci. U. S. A.* **104**, 1661–1666
55. Zhang, Z., and Zhang, R. (2008) Proteasome activator PA28 gamma regulates p53 by enhancing its MDM2-mediated degradation. *EMBO J.* **27**, 852–864
56. Soares, T. R., Reis, S. D., Pinho, B. R., Duchen, M. R., and Oliveira, J. M. A. (2019) Targeting the proteostasis network in Huntington's disease. *Ageing Res. Rev.* **49**, 92–103
57. Pratt, G., and Rechsteiner, M. (2008) Proteasomes cleave at multiple sites within polyglutamine tracts: activation by PA28gamma(K188E). *J. Biol. Chem.* **283**, 12919–12925
58. Unno, M., Mizushima, T., Morimoto, Y., Tomisugi, Y., Tanaka, K., Yasuoka, N., *et al.* (2002) The structure of the mammalian 20S proteasome at 2.75 Å resolution. *Structure* **10**, 609–618
59. Choi, W. H., de Poot, S. A. H., Lee, J. H., Kim, J. H., Han, D. H., Kim, Y. K., *et al.* (2016) Open-gate mutants of the mammalian proteasome show enhanced ubiquitin-conjugate degradation. *Nat. Commun.* **7**, 10963
60. Le Feuvre, A. Y., Dantas-Barbosa, C., Baldin, V., and Coux, O. (2009) High yield bacterial expression and purification of active recombinant PA28αβ complex. *Protein Expr. Purif.* **64**, 219–224
61. Pettersen, E. F., Goddard, T. D., Huang, C. C., Meng, E. C., Couch, G. S., Croll, T. I., *et al.* (2021) UCSF ChimeraX: structure visualization for researchers, educators, and developers. *Protein Sci.* **30**, 70–82